Control Strategy of a Five-Phase Induction Machine Supplied by the Current Source Inverter With the Third Harmonic Injection

Marcin Morawiec, *Senior Member, IEEE*, and Filip Wilczyński

***Abstract*—In the five-phase induction machine (IM), it is possible to better use the electromagnetic circuit than in the three-phase IM. This requires the use of an adequate converter system which will be supplied by an induction machine. The electric drive system described, in this article, includes the five-phase induction machine supplied by the current source inverter (CSI). The proposed novelty—not presented previously—is the control system structures for the five-phase IM, which is supplied by CSI. The proposed control systems allow for independent control of IM state variables in the first and the second system plane to inject the third harmonic. However, the third harmonic must be suitably associated with the fundamental harmonic. In the proposed solution, the machine vector model is not transformed into the (d–q) coordinate system that is connected to the rotor flux vector but utilizes the stationary system (α–β). The nonlinear model linearization is based on the demonstrated nonlinear variables transformation for i-orthogonal (α–β) (i) planes. Voltage control is applied to the control system structure. The control variables of the five-phase IM are the voltage in the dc link and the angular speed of the output current vector. In the control strategy, the control variables are determined for both system planes. Therefore, the transformation of these control variables to the dc link of CSI is proposed. The proposed control structure allows for independent control of variables in the first and second system planes. It leads to the possibility to increase the value of electromagnetic torque up to 12% for the five-phase IM, which has not been used before in the case of the machine supplied by the CSI. All theoretical issues are confirmed by experimental tests in the 5.5 kW five-phase IM.**

***Index Terms*—Electric machines, machine vector control, nonlinear control systems.**

I. Introduction

THE controlling idea of a five-phase induction motor (IM) is from 1969 [1]. The main advantages of multi (five) phase drives compared to their three-phase counterparts are [1]–[4]: better stator material utilization; lower rated current per phase; and greater reliability that means the ability to operate during an open phase fault and the possibility to increase the value of electromagnetic torque up to about 10%–12% [1], [3]–[7]. The concept of the control of the five-phase machine is based on the conjunction of two virtual machines in one single physical motor, for the reason that these machines ensure a higher value of torque generation by the fundamental and third-current harmonics utilization—in the case of the five-phase IM [6]. The main application field of the five-phase IM can be a drive system, e.g., electromobility (electric vehicles), electric aircraft (drones) or ship propulsion, and electric traction drives.

In the literature [1]–[15], there are a few significant control systems of multiphase IM, especially supplied by a voltage source inverter (VSI). The most popular control structures are based on the field-oriented control (FOC) in which the state variables of IM are oriented in the (d–q) coordinate system connected to the rotor flux vector. This approach was described in the literature by Salehifar *et al.* [8] and Wilczynski *et al.* [12]. In [13] and [14], the control system based on the FOC [24] and backstepping technique was shown. An alternative to FOC is the direct torque control (DTC) [15], [16], [25], which was adapted to multiphase machines. However, better properties of the control system can be achieved, when a transformation of nonlinear state variables of IM to a linear form is applied [26], [27]. The use of such an input–output linearization [17] was presented in [18] for multiphase IM.

In the state-of-the-art described in articles [1], [4], and [6], the control systems of a multiphase IM supplied mainly by the VSI are presented. The development of power electronic transistors has caused that the VSI-based structures are the most popular, and in over 30 years, they have better properties than the CSIs. However, in the literature [20]–[22], more and more often the articles about new power electronic components for the CSI mention the solution and the possibility of their "reactivation" as well as their different applications [22], [23] can be found. The main properties of using the CSI electric drives are the "almost" sinusoidal fundamental harmonic of the stator current and voltage, no-stress of the stator voltage *du/dt* as well as the possibility of long cable connected to the machine without the stator overvoltages. These properties of the CSI drives cause that the subject of the research on the development of electric drives toward multiphase is still actual, undiscovered, and interesting.

The formulated problem in this article concerns the control structure of the five-phase IM supplied by the CSI in which the two control system planes are introduced. The first system plane is responsible for the generation of fundamental harmonic.

Manuscript received July 19, 2021; revised November 9, 2021; accepted January 21, 2022. Date of publication February 7, 2022; date of current version April 28, 2022. This work was supported by the National Science Centre of Poland under Grant 2018/31/N/ST7/03889. Recommended for publication by Associate Editor J. He. *(Corresponding author: Marcin Morawiec.)*

The authors are with the Department of Electric Drives and Energy Conversion, Politechnika Gdanska, 80-233 Gdansk, Poland (e-mail: marcin.morawiec@pg.edu.pl; filip.wilczynski@pg.edu.pl).

Color versions of one or more figures in this article are available at https://doi.org/10.1109/TPEL.2022.3148526.

Digital Object Identifier 10.1109/TPEL.2022.3148526

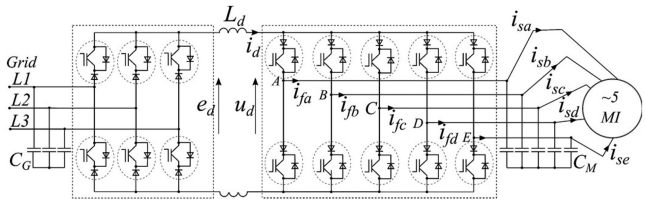

Fig. 1. Drive system with five-phase IM supplied by the CSI.

To increase the value of electromagnetic torque, the second system plane is used. As shown in [28]–[31], it is possible to control five-phase IM supplied by the CSI to generate only the fundamental harmonic—through this, the third harmonic is eliminated by the proper modulation algorithm of transistors in the CSI. However, to better use the magnetic circuit of five-phase IM, the third harmonic should be suitably controlled. If not, it should be compensated by a modulation algorithm in the CSI, as given in [28]–[31], without generating additional losses in the machine [6]. It is worth noting that if the five-phase machine is supplied by a voltage source (for example, the five-phase autotransformer), then the first and second harmonics are not synchronized and the losses in the machine are increased (see [1], [4], [6], and [28]–[31]).

In state-of-the-art presented in [1], [4], and [6], there is a lack of solution of control strategy in which the variables in the first and the second system plane are synchronized and controlled independently. In the literature [1]–[15], only the solutions for the five-phase machine supplied by the VSI are known. In [28]–[31], the vector control of five-phase IM in which the sinusoidal stator phase voltage and currents waveform is shaped (without third harmonic injection)—the third harmonic is reduced by the SVM algorithm. It is important to present the solution of the control strategy in which the electromagnetic torque of the five-phase IM supplied by the CSI is enhanced. Therefore, the main contribution of this article is to present the new control strategy which contains the two control system structures of the five-phase IM.

1) The rotor flux vector orientation of the state variables of IM—the FOC control structure for the first and second system planes.
2) The transformation of state variables of IM supplied by the CSI for the first and second system planes.

In the proposed solution of the control structures to reduce power losses in the CSI transistor bridge as well as in the dc link, the dc link current is not stabilized on the constant value. In the control systems, it is provided that the dc-link current is associated with the value of electromagnetic torque in the first and second system planes by introducing an additional factor. The control variables are the voltage e_d marked in Fig. 1 as the input to the dc link and the angular speed ω_{if} of output current vector, as shown in Fig. 1 as $\boldsymbol{i}_f\,(i_{fa,b,c,d,e})$. These control variables are obtained under classical feedback control laws for the first and second system planes presented in Section III, using the introduced state variables transformation. Therefore, in Section III, voltage—marked in Fig. 1 as e_d—is proposed to be split as $e_{d(1)}$ and $e_{d(2)}$, which means that $e_{d(1)}$ is obtained in the first system plane and $e_{d(2)}$ for the second system plane. It is worth noticing that $e_{d(2)}$ can be treated as the virtual control variable (virtual voltage, which in the CSI circuit does not exist because there is only one dc-link circuit). The proposed feedback control law contains the additional factor that allows maintaining the reference input values to the system as well as decoupling in the control paths of electromechanical and electromagnetic variables. The proposed solutions have never been presented before for the five-phase machine supplied by the CSI. It gives possibilities of independent generation of the first and third harmonics—to better use the electromagnetic circuit of the five-phase machine.

II. Problem Formulation

A. Electric Drive Scheme

The electric drive scheme is presented in Fig. 1. There is the controlled voltage source e_d, which can be realized by the three-phase current source rectifier [26], the dc-link circuit with the inductor L_d, ten transistors with the series-connected diodes bridge, and the output capacitors C_M.

The control variables in the drive system presented in Fig. 1 can be the output current vector components $i_{f\alpha(i)}$, $i_{f\beta(i)}$, or the input voltage $e_{d,}$ and the output current vector angular speed $\omega_{if(i)}$, which will be explained in the following sections.

B. Mathematical Model of the Five-Phase Machine

The five-phase reference coordinate system (*a-b-c-d-e*) can be transformed into two independent, stationary orthogonal planes: $\alpha_{(1)}$-$\beta_{(1)}$ and $\alpha_{(2)}$-$\beta_{(2)}$ [1]–[7]. As a result of the transformation, state vector variables are obtained in two planes associated with the first—fundamental—and third harmonic, respectively. The differential equations of the mathematical model for the stator current and rotor flux vectors have the form [18]

$$\frac{d\boldsymbol{i}_{s(i)}}{d\tau} = a_{1(i)}\boldsymbol{i}_{s(i)} + a_{2(i)}\psi_{r(i)} + ja_{3(i)}\omega_{r(i)}\psi_{r(i)} + a_{4(i)}u_{s(i)} \tag{1}$$

$$\frac{d\psi_{r(i)}}{d\tau} = a_{5(i)}\boldsymbol{i}_{s(i)} + a_{6(i)}\psi_{r(i)} + j\omega_{r(i)}\psi_{r(i)} \tag{2}$$

$$\frac{d\omega_r}{d\tau} = \frac{1}{J}\left(\sum_{i=1}^{N} T_{e(i)} - T_L\right) \tag{3}$$

where $i = 1$ or 2, and $\boldsymbol{i}_{s(i)}$, $\boldsymbol{u}_{s(i)}$, and $\psi_{r(i)}$ are the stator current, stator voltage, and rotor flux vectors, respectively, and J is the system inertia. $T_{e(i)}$ is the torque generated in the ith plane and is defined as follows:

$$T_{e(i)} = a_{7(i)}\mathrm{Im}(\psi^*_{r(i)}\mathrm{i}_{s(i)})\,. \tag{4}$$

For simplification, other coefficients are introduced as

$$a_{1(i)} = -(R_{s(i)}L^2_{r(i)} + R_{r(i)}L^2_{m(i)})/L_{r(i)}w_{\sigma(i)}$$
$$a_{7(i)} = L_{m(i)}/L_{r(i)}$$
$$a_{3(i)} = L_{m(i)}/w_{\sigma(i)}, \quad a_{2(i)} = R_{r(i)}L_{m(i)}/L_{r(i)}w_{\sigma(i)}$$
$$a_{4(i)} = L_{r(i)}/w_{\sigma(i)}$$

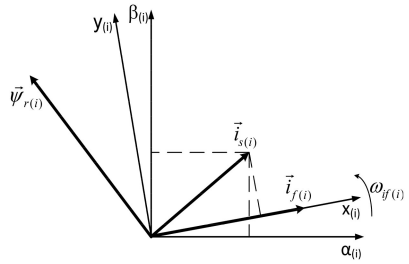

Fig. 2. Variables in $(\alpha_{(i)}$–$\beta_{(i)})$ stationary system and in $(x_{(i)}$–$y_{(i)})$ associated with the output current vector $\boldsymbol{i}_{f(i)}$ defined in [13].

$$a_{5(i)} = R_{r(i)}L_{m(i)}/L_{r(i)},\ a_{6(i)} = -R_{r(i)}/L_{r(i)}$$
$$w_{\sigma(i)} = L_{r(i)}L_{s(i)} - L^2_{m(i)}$$

stator and rotor resistances are denoted by R_s, R_r, self-inductance by L_s, L_r, and mutual inductance by L_m, respectively.

C. Mathematical Model of IM in (x–y) Coordinate System

For the control system design of IM supplied by the CSI, it is better to associate the vectors of the five-phase IM with the (*x*–*y*) coordinate system (see Fig. 2). Then, the five-phase IM model in (*x*–*y*) coordinate system has the following form:

$$\frac{di_{sx(i)}}{d\tau} = a_{1(i)}i_{sx(i)} + a_{2(i)}\psi_{rx(i)} + \omega_{if(i)}i_{sy(i)} + \omega_{r(i)}a_{3(i)}\psi_{ry(i)} + a_{4(i)}u_{sx(i)} \tag{5}$$

$$\frac{di_{sy(i)}}{d\tau} = a_{1(i)}i_{sy(i)} + a_{2(i)}\psi_{ry(i)} - \omega_{if(i)}i_{sx(i)} - \omega_{r(i)}a_{3(i)}\psi_{rx(i)} + a_{4(i)}u_{sy(i)} \tag{6}$$

$$\frac{d\psi_{rx(i)}}{d\tau} = a_{6(i)}\psi_{rx(i)} + (\omega_{if(i)} - \omega_{r(i)})\psi_{ry(i)} + a_{5(i)}i_{sx(i)} \tag{7}$$

$$\frac{d\psi_{ry(i)}}{d\tau} = a_{6(i)}\psi_{ry(i)} - (\omega_{if(i)} - \omega_{r(i)})\psi_{rx(i)} + a_{5(i)}i_{sy(i)} \tag{8}$$

$$\frac{d\omega_{r(i)}}{d\tau} = \frac{L_m}{JL_r}\left(\sum_{i=1}^{2}(\psi_{rx(i)}i_{sy(i)} - \psi_{ry(i)}i_{sx(i)})\right) - \frac{1}{J}T_{L(i)} \tag{9}$$

where $\omega_{if(i)}$ is the angular speed of the (*x*–*y*) coordinate frame.

D. Mathematical Model of CSI

According to the designation in Fig. 1, the dc link and the output capacitors can be described [26]–[31] as follows:

$$\frac{di_d}{d\tau} = \frac{1}{L_d}(e_d - R_d i_d - u_d) \tag{10}$$

$$\frac{du_{sx(i)}}{d\tau} = \frac{1}{C_M}\left(i_{fx(i)} - i_{sx(i)}\right) + \omega_{if}u_{sy(i)} \tag{11}$$

$$\frac{du_{sy(i)}}{d\tau} = \frac{1}{C_M}(i_{fy(i)} - i_{sy(i)}) - \omega_{if}u_{sx(i)} \tag{12}$$

where $\omega_{if(i)}$ is the angular speed of $x_{(i)}$–$y_{(i)}$ coordinate system, $u_{cx(i)}$ and $u_{cy(i)}$ are the components of output capacitor voltage, $i_{fx,y(i)}$ is output current vector components, and R_c is the series resistance of output capacitor C_M.

The module of output current vector can be defined as follows:

$$i_{f(i)} = i_d K \tag{13}$$

where K factor ensures the proper value of the current i_d in the dc link during the output power ratio changes, and for the two system planes ($i = 0, 1$), it can be defined as

$$K = 1 - \frac{p_{s(i+1)}}{p_{s(i)}} \tag{14}$$

$$p_{s(i)} = u_{sx(i)}i_{sx(i)} + u_{sy(i)}i_{sy(i)},\ i = 0,\ 1 \text{ and } p_{s(i)} \neq 0 \tag{15}$$

where $i = 0$ means first system plane and $i = 1$ means second system plane.

It is worth mentioning that if the output current vector is generating only in the single plane (e.g., in the first system plane), then $p_{s(i+1)} = 0$ and $K = 1$. The same case is when the output current vector is generated only in the second system plane, then K must be equal to 1.0 (taking into account that $p_{s(i)} << p_{s(i+1)}$) or it can be assumed that $K = 1 - p_{s(i+1)}$ for $p_{s(i)} << p_{s(i+1)}$.

Assumption: In the electric drive system presented in Fig. 1, it is possible to develop such a control system, which allows decomposing the nonlinear model (5)–(12) by using a proper transformation into the two subsystems. Furthermore, it is possible to independently control state variables in both system planes (first and second) of five-phase IM to better use the electromagnetic circuit.

III. Control System of Electric Drive Supplied by the CSI

The mathematical model of the drive system with the five-phase IM (5)–(9) and the CSI (10)–(12) is strongly nonlinear. Therefore, in the literature [17], [18], and [32], the input–output linearization of the state variables is proposed or the use of the multiscalar variables is proposed in [36]. From the point of view of the feedback control law as well as the control structure, it is beneficial to consider the $x_{(i)}$–$y_{(i)}$ coordinate system oriented with the output current vector $\boldsymbol{i}_{f(i)}$ of the CSI in which the following occurs:

$$i_{fx(i)} = i_d K \text{ and } i_{fy(i)} \approx 0 \tag{16}$$

and the angular speed of the output current vector is $\omega_{if(i)}$.

To obtain the linearization control law, for the mathematical model of five-phase IM supplied by the CSI (5)–(12), the transformation has the following form:

$$x_{11(i)} = \omega_{r(i)} \tag{17}$$

$$x_{12(i)} = -x_{41(i)}\psi_{ry(i)} - \omega_{if(i)}C_{M(i)}x_{32(i)} \tag{18}$$

$$x_{21(i)} = \psi^2_{rx(i)} + \psi^2_{ry(i)} \tag{19}$$

$$x_{22(i)} = x_{41(i)}\psi_{rx(i)} + \omega_{if(i)}C_{M(i)}x_{31(i)} \tag{20}$$

$$x_{31(i)} = \psi_{rx(i)} u_{sy(i)} - \psi_{ry(i)} u_{sx(i)} \tag{21}$$

$$x_{32(i)} = \psi_{rx(i)} u_{sx(i)} + \psi_{ry(i)} u_{sy(i)} \tag{22}$$

$$x_{41(i)} = i_{fx(i)} \tag{23}$$

$$x_{42(i)} = i_{fy(i)} \tag{24}$$

where $x_{(i)} = [x_{11(i)}, x_{12(i)}, x_{21(i)}, x_{22(i)}, x_{31(i)}, x_{32(i)}, x_{41(i)}, x_{42(i)}]$.

The linearization variables (17)–(24) are introduced by using the general form [36] and the assumption; its derivative does not change, therefore, $du_{s(i)}/d\tau \approx 0$ (in a small period), so it can be assumed that

$$i_{sx(i)} \approx i_{fx(i)} + \omega_{if(i)} C_{M(i)} u_{sy(i)} \tag{25}$$

$$i_{sy(i)} \approx -\omega_{if(i)} C_{M(i)} u_{sx(i)} \tag{26}$$

in $x_{(i)}$–$y_{(i)}$ coordinate system.

By using (17)–(24) and (5)–(12), the new system in $x_{(i)}$ has the following form:

$$\dot{x}_{11(i)} = x_{12(i)} \tag{27}$$

$$\dot{x}_{12(i)} = \frac{1}{T_{(i)}}(-x_{12(i)} + m_{1(i)}) \tag{28}$$

$$\dot{x}_{21(i)} = a_{6(i)} x_{21(i)} + 2a_{5(i)} x_{22(i)} \tag{29}$$

$$\dot{x}_{22(i)} = \frac{1}{T_{(i)}}(-x_{22(i)} + m_{2(i)}) \tag{30}$$

$$\dot{x}_{31(i)} = \left(\omega_{if(i)}^2 - \omega_{if(i)} x_{11(i)}\right) x_{31(i)} - \omega_{if(i)} \left(a_{5(i)} x_{32(i)} + a_{6(i)} p_{s(i)}\right) \tag{31}$$

$$\dot{x}_{32(i)} = \left(\omega_{if(i)}^2 - \omega_{if(i)} x_{11(i)}\right) x_{32(i)} + \omega_{if} \left(a_{6(i)} x_{31(i)} + a_{5(i)} q_{s(i)}\right) \tag{32}$$

$$\dot{x}_{41(i)} = \frac{K}{L_d}(e_{d(i)} - u_{sx(i)}) - \frac{R_d}{L_d} x_{41(i)} \tag{33}$$

$$\dot{x}_{42(i)} = 0 \tag{34}$$

in which the nonlinear terms are

$$m_{1(i)} = T_{i(i)} \left(-x_{11(i)} x_{22(i)} - a_{5(i)} i_{sy(i)} x_{41(i)} + \frac{K}{L_d} u_{sx(i)} \psi_{ry(i)} + v_{1(i)}\right) \tag{35}$$

$$m_{2(i)} = T_{i(i)} \left(x_{11(i)} x_{12(i)} + a_{5(i)} (x_{12(i)}^2 + x_{22(i)}^2)/x_{21(i)} - \frac{K}{L_d} u_{sx(i)} \psi_{rx(i)} + v_{2(i)}\right) \tag{36}$$

and

$$v_{1(i)} = -\frac{K}{L_d} e_{d(i)} \psi_{ry(i)} + \omega_{if(i)} \Gamma_{1(i)} \tag{37}$$

$$v_{2(i)} = \frac{K}{L_d} e_{d(i)} \psi_{rx(i)} + \omega_{if(i)} \Gamma_{2(i)} \tag{38}$$

$q_{s(i)} = i_{sx(i)} u_{sy(i)} - i_{sy(i)} u_{sx(i)}$ and $p_{s(i)}$ is defined in (15).

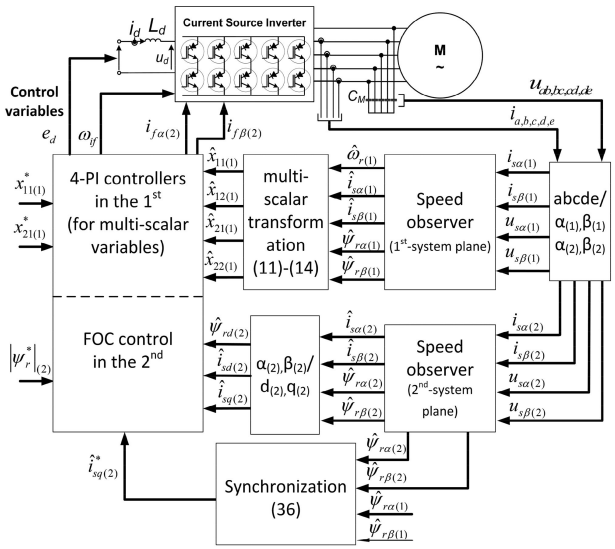

Fig. 3. Control system structure with the proposed voltage approach with controls e_d and $\omega_{if(1,2)}$ presented in Section III.

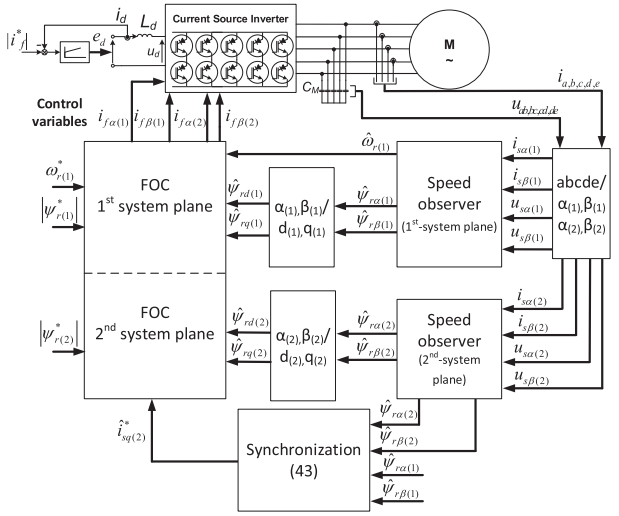

Fig. 4. Control system structure with the FOC of five-phase IM.

The state feedback linearizing control variables can be determined from (35) and (36)

$$v_{1(i)} = x_{11(i)} x_{22(i)} + a_{5(i)} i_{sy(i)} x_{41(i)} - \frac{K}{L_d} u_{sx(i)} \psi_{ry(i)} + \frac{1}{T_{i(i)}} m_{1(i)} \tag{39}$$

$$v_{2(i)} = -x_{11(i)} x_{12(i)} - a_{5(i)} (x_{12(i)}^2 + x_{22(i)}^2)/x_{21(i)} + \frac{K}{L_d} u_{sx(i)} \psi_{rx(i)} + \frac{1}{T_{i(i)}} m_{2(i)} \tag{40}$$

where $m_{1(i)}$ and $m_{2(i)}$ are the new controls, as shown in Fig. 17.

The control variables in the drive system can be determined from (37) and (38)

$$e_{d(i)} = \frac{L_d (v_{2(i)} \Gamma_{1(i)} - v_{1(i)} \Gamma_{2(i)})}{K(\psi_{rx(i)} \Gamma_{1(i)} + \psi_{ry(i)} \Gamma_{2(i)})} \tag{41}$$

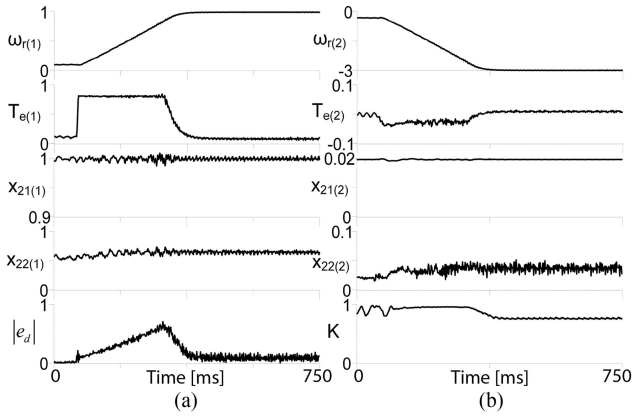

Fig. 5. Machine is starting-up to 1.0 p.u., the following variables are presented. (a) Equations (19) and (20) $T_{e(1)}$ and the control variable (41) in the first plane. (b) Electromagnetic torques $T_{e(2)}$ and factor *K*.

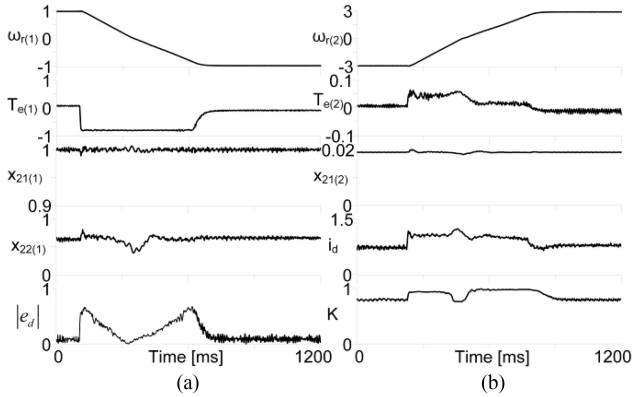

Fig. 6. Machine is reversing to −1.0 p.u., the following variables are presented. (a) Equations (19) and (20) and the control variable (41) in the first plane. (b) Equations (19) and (20) for the second plane and electromagnetic torques $T_{e(1,\ 2)}$ (4) and factor *K*.

$$\omega_{if(i)} = \frac{v_{1(i)}\psi_{rx(i)} + v_{2(i)}\psi_{ry(i)}}{K(\psi_{rx(i)}\Gamma_{1(i)} + \psi_{ry(i)}\Gamma_{2(i)})} \tag{42}$$

where

$$\left(\psi_{rx(i)}\Gamma_{1(i)} + \psi_{ry(i)}\Gamma_{2(i)}\right) \neq 0$$

$$\Gamma_{1(i)} = x_{22(i)} - \frac{R_d}{L_d}C_{M(i)}x_{32(i)} - C_{M(i)}a_{6(i)}p_{s(i)} \tag{43}$$

$$\Gamma_{2(i)} = -x_{12(i)} + \frac{R_d}{L_d}C_{M(i)}x_{31(i)} + C_{M(i)}a_{6(i)}q_{s(i)}\,. \tag{44}$$

It is worth noticing that (31)–(34) represent the dynamics, which have been made unobservable from the assumed outputs $\omega_{r(i)}$ and $\psi^2_{rx(i)} + \psi^2_{ry(i)}$ by the state feedback control variables (41), (42). Hence, in the control structure, the structure with the four PI controllers of the variables defined in (17)–(20) for the first system plane (see Fig. 17) can be used.

In the control system structure of the five-phase IM supplied by the CSI, it is necessary to synchronize the two system planes. In the literature [9]–[15] and [33], a few methods of synchronization are proposed. The third harmonic should be

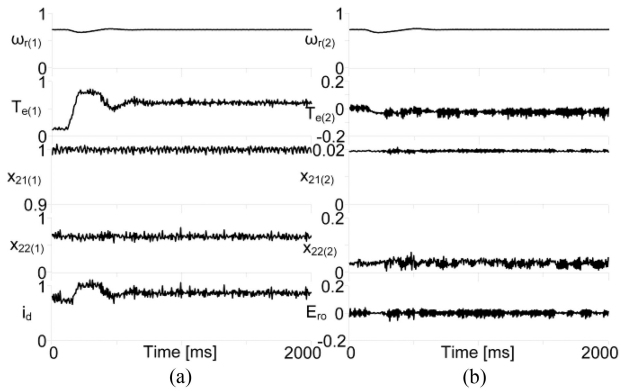

Fig. 7. Machine is loaded to −1.0 p.u., the following variables are presented. (a) Equations (19) and (20), $T_{e(1)}$ in the first plane and current i_d. (b) Equations (19) and (20), electromagnetic torques $T_{e(2)}$, and synchronization error defined in (49).

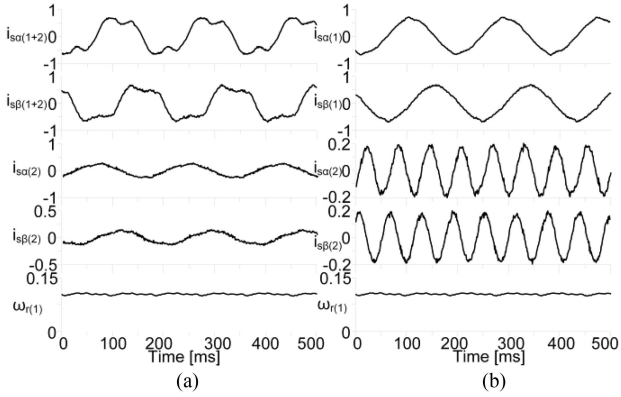

Fig. 8. Stationary state, the variables are presented: Stator current vector $i_{s\alpha,\beta}$ in the first and second system plane as well as the rotor speed are presented. (a) Third harmonic is injected together with the fundamental. (b) Only fundamental harmonic is generated.

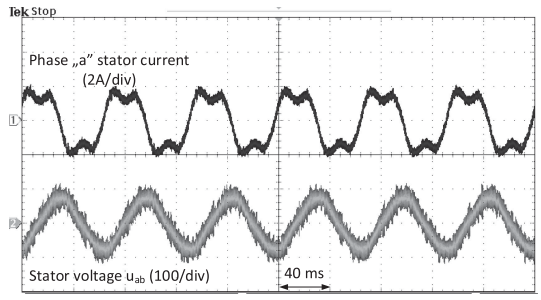

Fig. 9. Stator current and stator voltage waveforms, the third harmonic is injected together with the fundamental.

aligned with the fundamental harmonic of the rotor flux vector (by the alignment of the rotor flux vector angles θ_{e2} to θ_{e1}). This alignment can be provided by using the one *P*–controller and the dependence presented in [33]

$$i^{eq}_{sq(2)} = -3\frac{R_{r(1)}L_{m(1)}R_{r(2)}L_{m(2)} + L_{r(2)}L_{r(1)}}{L_{r(1)}R_{r(2)}L_{m(2)}}i_{sq(1)}$$

$$i^{*}_{sq(2)} = k_q(\theta_{e1} - \theta_{e2}) + i^{eq}_{sq(2)},\ k_q > 0 \tag{45}$$

or by using two–PI controllers structure, such as in [34].

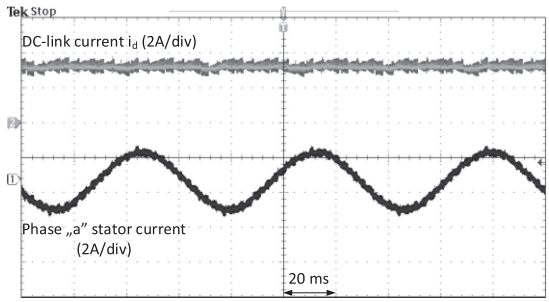

Fig. 10. Current i_d in the dc link and stator current waveforms, in the case of the fundamental harmonic, is generated only (the third harmonic is not injected), the motor is not loaded.

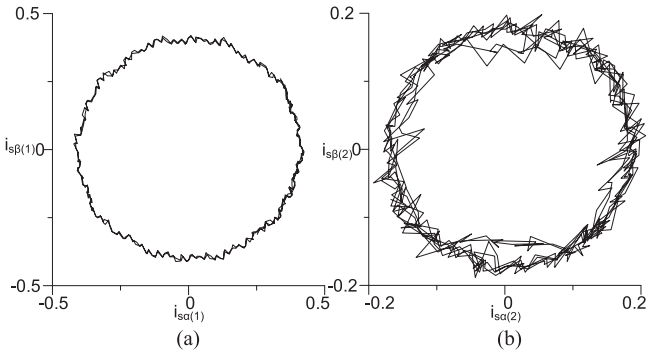

Fig. 11. Stator current vector components (measured by the transducer) in (a) $(\alpha_{(1)} - \beta_{(1)})$ and (b) $(\alpha_{(2)} - \beta_{(2)})$ in per-unit. The third harmonic is injected.

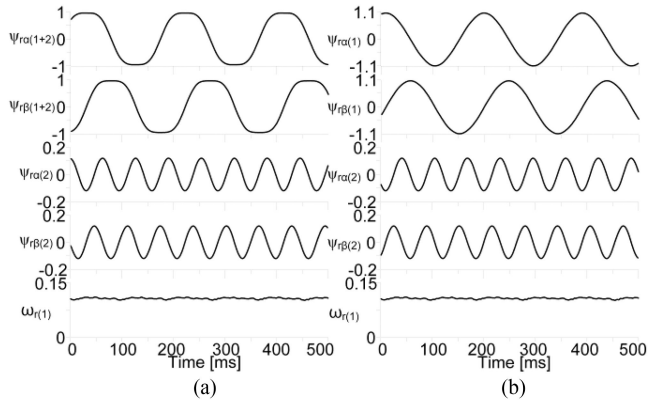

Fig. 12. Rotor speed $\omega_{r(1)}$ and rotor flux vector components $\psi_{r\alpha,\beta(1+2)}$, $\psi_{r\alpha,\beta(1)}$, $\psi_{r\alpha,\beta(2)}$ in (a) $(\alpha_{(1)} - \beta_{(1)})$ and (b) $(\alpha_{(2)} - \beta_{(2)})$. The third harmonic is injected.

We propose to introduce the new synchronization scheme in which the multiscalar variables are used. The position of the rotor flux vector can be determined as follows:

$$\theta_{e2} = \tan^{-1}\left(\psi_{ry}/\psi_{rx}\right) \tag{46}$$

and by using (7) and (8), the derivative of θ_{e2} has the following form:

$$\frac{d\theta_{e2}}{d\tau} = \omega_{r(2)} + \frac{a_{5(2)}x_{12(2)}}{x_{21(2)}},\ x_{21(2)} \neq 0. \tag{47}$$

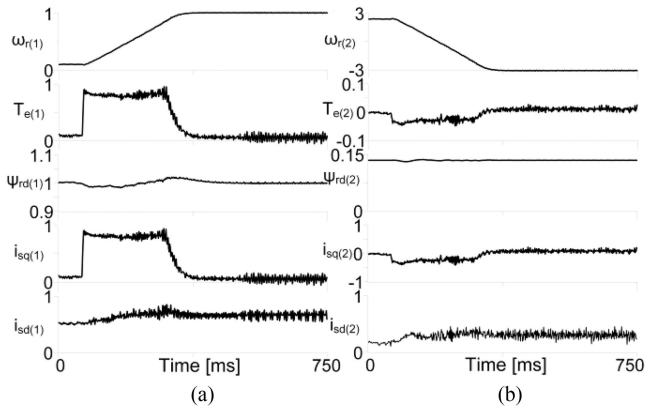

Fig. 13. Machine is starting-up to 1.0 p.u., the variables are presented: the rotor speed ω_r, electromagnetic torque (4), rotor flux vector module ψ_{rd}, and stator current vector components $i_{sd,q}$. (a) For the first plane. (b) For the second system plane.

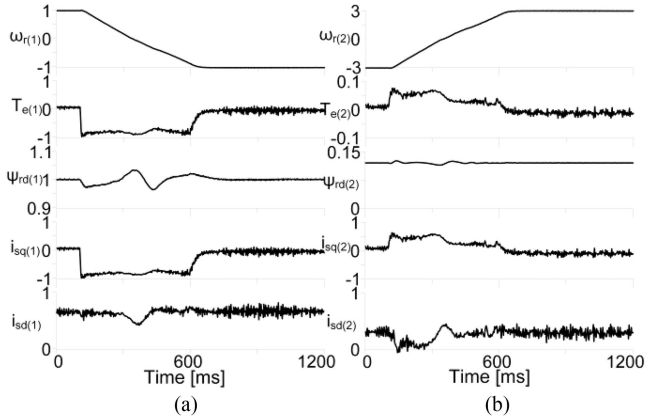

Fig. 14. Machine is reversing to -1.0 p.u., the variables are presented: the rotor speed ω_r, electromagnetic torque (4), rotor flux vector module ψ_{rd}, and stator current vector components $i_{sd,q}$. (a) For the first plane. (b) For the second system plane.

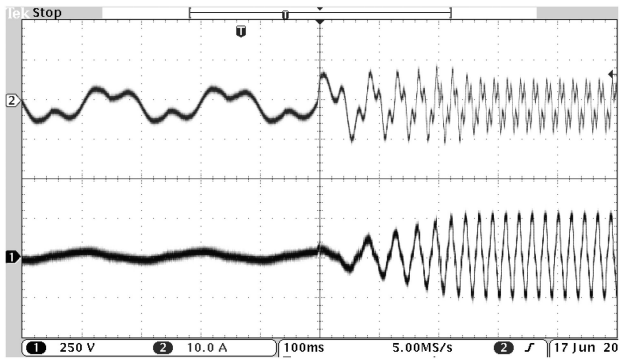

Fig. 15. Stator current and voltage during the machine start-up to 1.0 (channel 1—stator voltage u_{ab} and channel 2—phase "a" stator current).

State feedback linearizing control for (47) can be determined as

$$x^*_{12(2)} = \frac{1}{T_\theta}\left(m_3 - \omega_{r(2)}\right) \tag{48}$$

where $\frac{1}{T_\theta} \approx a_{5(2)}$ for $x_{21(2)} << |\psi_{r(2)}|$.

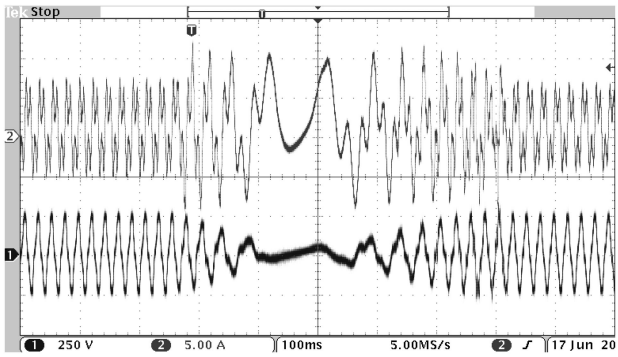

Fig. 16. Stator current and voltage during the machine reversing from −1.0 to 1.0 p.u. (channel 1—stator voltage u_{ab} and channel 2—phase "a" stator current).

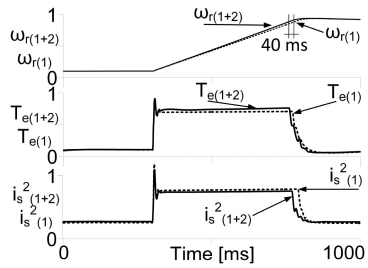

Fig. 17. Comparison test during the IM is starting-up to 0.9 p.u. The rotor speed, electromagnetic torque, and square of stator current are presented.

Here, m_3 is the output from the PI-controller in which the input is $E_{ro} = \theta_{e1} - \theta_{e2}$. The value of m_3 is determined as follows:

$$m_3 = k_p(\theta_{e1} - \theta_{e2}) + k_i \int_{t_0}^{t_1} (\theta_{e1} - \theta_{e2}) d\tau \qquad (49)$$

where k_p and k_i are the tuning gains defined in Table II, and t_0-t_1 is an integration period.

IV. Control Strategy of the Electric Drive Supplied by the CSI

The control strategies of the IM supplied by the CSI are known in the literature [24]–[31] and can be divided into two groups. The first one is based on *current* control. There are the FOC control structures in which the linearizing of IM control variables are the stator current vector components $i^*_{s\alpha,\beta}$ or the output current vector $i^*_{f\alpha,\beta}$. The second control structure is named *voltage* control, and the state feedback linearizing control variables are the input voltage e_d and angular speed ω_{if} of output current vector $\boldsymbol{i}_f$ (see Section III). In this article, two control system structures are analyzed and compared. The first one is based on the solution, proposed in Section III, with the multiscalar transformation, and the second is based on the classical FOC control system for the first and the second system plane. In this section, both control system structures are shown and discussed.

Fig. 3 presents the control structure with the proposed in (17)–(24) new state of variables and feedback control laws (35)–(42). There are blocks of the speed observer [35], transformation (17)–(24), synchronization (48), (49), and measurements (Park transformation). The control systems from Figs. 3 and 4 can be named "sensorless" because the rotor speed value is not measured but estimated in the observer structure [35] in the first system plane. In the second system plane, the classical flux observer structure is applied. In the control structure from Fig. 3, the control variables are the voltage $e_{d(1)}$ and $\omega_{if(1)}$, whose values are calculated in the first system plane. In the second system plane, the control variables $e_{d(2)}$ and $\omega_{if(2)}$ are

TABLE I
Comparison of Selected Properties of the Proposed Control Structures

Name	Voltage control structure from Fig.3	FOC structure from Fig. 4
Possible to inject the third harmonic	Yes	Yes
Oscillation of state variables of IM in the dynamic states	Small	High
Oscillation of state variables of IM in the stationary states	Very small	Medium
Decoupled control law	Yes	No
Coupling between electromechanic and electromagnetic control paths (during the dynamic states)	No	Yes
Value of the level of oscillations during the stationary state	< 0.015 p.u.	> 0.08 p.u.
Max. value of synchronization error during a dynamic states	< 0.02 p.u.	< 0.02 p.u.
Dynamic and control possibility	100 %	100 %
The rising time during the starting to nominal speed	0.3 s	0.3 s
Setting time during the starting to nominal speed	< 0.1 s	< 0.1 s
Tracking error of rotor speed in the stationary state	< 0.05 p.u.	< 0.05 p.u.
Tracking error of rotor flux vector module in the stationary state	< 0.015 p.u.	< 0.02 p.u.
The complexity of implementation and tuning	High	Medium

TABLE II
Initial Values of PI-Controllers

Symbol	Quantity	Values
$k_{p11(1)}$, $k_{i11(1)}$	tuning gain of variable $x_{11(1)}$	15; 0.01 p.u.
$k_{p12(1)}$, $k_{i12(1)}$	tuning gain of variable $x_{12(1)}$	5; 0.5 p.u.
$k_{p21(1)}$, $k_{i21(1)}$	tuning gain of variable $x_{21(1)}$	5; 0.01 p.u.
$k_{p22(1)}$, $k_{i22(1)}$	tuning gain of variable $x_{22(1)}$	5; 0.01 p.u.
$k_{p12(2)}$, $k_{i12(2)}$	tuning gain of variable $x_{12(2)}$	5; 0.5 p.u.
$k_{p21(2)}$, $k_{i21(2)}$	tuning gain of variable $x_{21(2)}$	5; 0.01 p.u.
$k_{p22(2)}$, $k_{i22(2)}$	tuning gain of variable $x_{22(2)}$	0.5; 0.001 p.u.
k_p, k_i	synchronization controller (49)	1.5; 0.001 p.u.
$k_{po(1)}$, $k_{io(1)}$	tuning gain of variable $\omega_{r(1)}$	1.0; 0.01 p.u.
$k_{p\psi r(1)}$, $k_{i\psi r(1)}$	tuning gain of variable $\psi_{r(1)}$	5; 0.01 p.u.
$k_{p\psi r(2)}$, $k_{i\psi r(2)}$	tuning gain of variable $\psi_{r(2)}$	7; 0.05 p.u.

determined. A characteristic feature of this control structure is that there is only one dc-link circuit with control variable e_d (see Fig. 1), which can be considered as the sum of both voltages determined in the first and second system planes

$$e_d = e_{d(1)} + e_{d(2)}\,. \tag{50}$$

Under this assumption (50), the "virtual" dc-link circuit for the second system plane is introduced. This means that the additional "virtual" circuit is used in the theoretical (mathematical) considerations to obtain the linearizing feedback control law in the second plane. According to the definition of factor K (14) and the output current (16), the variables (23) and (24) for the second system plane have the following form:

$$x_{41(2)} = i_{fx(2)} = (1-K)i_d \tag{51}$$

$$x_{42(2)} = 0 \tag{52}$$

which means that the current in the virtual dc-link circuit is $(1-K)$ smaller than the current i_d. By this, the reference output current vector in the second system plane (see Fig. 3) has the form

$$\left|i^*_{f(2)}\right| = \sqrt{\left(x^{*2}_{12(2)} + x^{*2}_{22(2)}\right)\Big/ x_{21(2)}}\;, \quad x_{21(2)} \neq 0 \tag{53}$$

where

$$x_{21(2)} = \psi^2_{rx(2)} + \psi^2_{ry(2)} \neq 0.$$

In Fig. 3, the first and second system blocks are determined by (35)–(42), which contain the cascaded connected four PI–controllers [26] (presented in detail in Fig. 17 of the Appendix). The synthesis of the PI-controller in the control structure of the five-phase IM has been presented in [15]. The same procedure can be applied to obtain the initial selection of the proportional and integrator coefficients of PI controllers. These coefficients are given in Table II.

The structure presented in Fig. 17 can be directly implemented in Fig. 3 for the first system plane; however, the second system plane should be synchronized to the first by using (48) and (49) and omitting $x_{11(2)}$ PI-controller (see Fig. 17) only forcing the value of $x^*_{12(2)}$ determined by (48).

The value of factor K is limited to the $K_{\max} = 1$ and $K_{\min}$ as a function of variables $K_{\min} = f(x_{12\,\lim(2)}, x_{22\,\lim(2)}, x_{21(2)}, i_{d\max}, i_d)$, where $x_{12\lim(2)}$ and $x_{22\lim(2)}$ are the maximum value of the variables $x_{12(2)}$ and $x_{22(2)}$, $i_{d\max}$ is the maximum value of current i_d. This prevents the unexpected states during the dynamic states of IM because of (14). $K_{\min}$ value can be obtained as follows:

$$K_{\min} = \sqrt{\frac{i^2_{d\max}x_{21(2)} - x^2_{12\,\lim(2)} - x^2_{22\,\lim(2)}}{i^2_d x_{21(2)}}} \tag{54}$$

and $x_{21(2)} > 0$ and $i_d > 0$.

Fig. 3 shows the control structure, which is particularly advantageous because the state variables can be controlled in both system planes independently. This control structure is more complicated than [13]–[16]. However, it is possible to increase the value of electromagnetic torque in the whole drive system. This feature is comparable to the drive system with a five-phase machine supplied by the VSI [1]–[7], [9], [10].

TABLE III
ELECTRIC DRIVE SYSTEM PARAMETERS AND REFERENCES UNIT

Symbol	Quantity	Values
	Five-phase Induction motor	
$R_{s(1,2)}$	stator resistance	0.02 p.u.
$R_{r(1,2)}$	rotor resistance	0.02 p.u.
$L_{m(1)}$	magnetizing inductance in first plane	2.04 p.u.
$L_{s(1)}$, $L_{r(1)}$	stator and rotor inductance in first plane	2.12 p.u.
$L_{s(2)}$, $L_{r(2)}$	stator and rotor inductance in second plane	0.92 p.u.
$L_{m(2)}$	magnetizing inductance in second plane	0.73 p.u.
P_n	nominal power	5.5 kW
I_n	nominal stator current (Y)	8.8 A
U_n	nominal stator voltage (Y)	173 V
n	nominal rotor speed	1440 r/min
f	nominal frequency	50 Hz
$U_b = U_n\sqrt{5}$	reference voltage	173 V
$I_b = I_n\sqrt{5}$	reference current	19.6 A
P_b	reference power	7.5 kW
	Current Source Inverter parameters	
	Switching frequency	3.3 kHz
	Capacitor	5 μF
	Inductor	10 mH
	Transistors model	MMG50SR120FZB

To compare the control structures and their properties, the control structure based on the FOC control is presented in Fig. 4. The control system is similar to classical control law, which is obtained by using the FOC [28] (for five-phase IM supplied by the CSI). However, in the structure presented in Fig. 4, in addition to the fundamental harmonic, it is possible to generate the third harmonic of output current (thereby increasing the electromagnetic torque). It is worth noticing that the control variables are the output current vector $i_{f\alpha,\beta}$ for the first and the second system planes (to obtain the value of the e_d the PI controller of the current i_d is applied with the reference value $|i^*_f| = \sqrt{i^2_{f(1)} + i^2_{f(2)}}$).

The indirect-FOC-based control systems for the five-phase machine supplied by the CSI are presented in [28] and, for a three-phase machine, they are well known in the literature. However, the control structure from [28] does not allow us to control variables in the second system plane. Therefore, in this article, we want to concentrate on the FOC control structure with the possibility of the third-harmonic injection.

V. EXPERIMENTAL RESULTS

The experimental tests were carried out on the 5.5 kW drive system with a five-phase IM with rated parameters: 173 V phase voltage; 8.8 A phase current; 1440 r/min; nominal torque of 36.5 N·m; and the current source converter. The control system was implemented in a microprocessor system with the floating-point digital signal processor (ADSP21363) with a sampling time of 150 μs. The inverter operates with a transistor switching frequency twice the control sampling time 3.3 kHz. The electric drive parameters are given in Table III.

The waveforms registered during performance tests are presented in Section V-A and B. The resolutions of registered waveforms are limited due to the date buffer in DSP (it is limited to up to 1000 points for one track). Waveforms presented in Figs. 9 and 10 as well as in Figs. 15 and 16 are registered using the digital oscilloscope with a resolution of up to 5 MS/s. In Section V-A, the waveforms for the control system structure are shown in Fig. 3. In Section V-B, the waveforms for the FOC control structure are shown in Fig. 4.

TABLE IV
THD OF STATOR CURRENT AND VOLTAGE

THD [%] Fundamental harmonic is generated			
	$T_L \approx 0.1$ p.u.	$T_L \approx 0.5$ p.u.	$T_L \approx 0.8$ p.u.
u_{sa}	5.5 %	1.8 %	1.1 %
i_{sa}	2.7 %	1.2 %	1.1 %
THD [%] Fundamental and third harmonic are generated			
	$T_L \approx 0.1$ p.u.	$T_L \approx 0.5$ p.u.	$T_L \approx 0.8$ p.u.
u_{sa}	5.4 %	1.9 %	1.2 %
i_{sa}	2.2 %	1.5 %	1.3 %

A. Voltage Control Structure With Controls E_d and $\omega_{\mathrm{if}(1,2)}$

Fig. 5 presents the tracking responses of the multiscalar variables (17)–(20) in ($\alpha_{(1)}$-$\beta_{(1)}$), electromagnetic torques $T_{e(1,\,2)}$ under the speed change from 0.1 to 1.0 p.u. The torque increases immediately (about 5 ms) up to an upper limit (0.8 p.u.), which underlines the effectiveness of the proposed control technique. The motor accelerates fast to attain the commanded value (in this case the machine is not loaded). In Fig. 5(b), the same variables are shown but for the second system plane as well as the factor *K*. Through this coefficient, the suitable properties of IM are provided and the dc-link current value guarantees the desired performance (desired reference value). Note that the current in dc link is proportional to the electromagnetic torque; through this, the power losses in the transistors are limited (see Fig. 5) which are not stabilized to the constant value.

The square of rotor flux (x_{21}) remains almost constant during the machine dynamic states. In Fig. 6, the same variables are presented as in Fig. 5, but during the IM reverse. The variable $T_{e(2)}$ has a value smaller than 0.07 in dynamic states, but the summarized value of electromagnetic torque is higher than in the case of a three-phase machine. Therefore, the five-phase machine start-up or reverse is achieved in a shorter time than in the case of a three-phase one. The value of electromagnetic torque is limited to 0.8 p.u. (through the $x{*}_{12(1)}$ value limit, Appendix).

The test from Fig. 6 presents the rotor speed smooth cross through zero to obtain the smallest rotor speed error (notice that, in the control structure, the state variables are reconstructed using the speed observer [35]). Near the zero speed, the oscillations of $x_{22(1,\,2)}$ are visible. The value of *K* is limited to 1.0, and $K_{\min}$ prevents the overcurrent in the dc link.

The load torque change is shown in Fig. 7. After 0.2 s, the load torque was activated to about 0.72 p.u. The five-phase machine was loaded with a dc machine. The proposed voltage control structure (see Fig. 3) with the multiscalar variables provides the decoupling of decomposed two subsystems, which is visible in Fig. 7. The multiscalar variables x_{21} and x_{22} remain almost constant during dynamic states of IM (see Figs. 5 and 7). This last advantage has an enormous influence on the whole electric drive performance properties as well as the stable work of the control system structure.

Fig. 8 presents the waveforms of stator current vector components in the first and second system planes. The third harmonic is generated together with the fundamental; therefore, the stator current vector components $i_{s\alpha(1+2)}$, $i_{s\beta(1+2)}$ are trapezoidal [see Fig. 8(a)]. If the fundamental harmonic is generated only, then the shapes of stator current vector components are almost sinusoidal [see Fig. 8(b)]. In both presented cases, the IM is not loaded. It is worth noticing that the stator current vector components $i_{s\alpha(1+2)}$ and $i_{s\beta(1+2)}$ are the sum of $i_{s\alpha(1)} + i_{s\alpha(2)}$ components and $i_{s\beta(1)}$ and $i_{s\beta(2)}$, $i_{s\beta(1)} + i_{s\beta(2)}$, respectively. To confirm the waveforms from Fig. 8, the waveforms of stator current i_a, stator voltage u_{ab} have been registered by a digital oscilloscope and presented in Fig. 9. The third harmonic is injected with the fundamental harmonic. The IM is not loaded. The registered resolution is 1 M points per second.

Fig. 10 presents the waveforms of the current i_d in dc link and stator current in phase "*a*," during the fundamental harmonic generation only (the third harmonic is not injected). For this case, the stator current in phase "*a*" has a sinusoidal shape with a small content of higher harmonics. The motor is not loaded. In Table IV, THD values for the stator current and voltage (phase *A*) are presented. In the case of generation of the reference inverter output current vectors in both planes, the third harmonic is not considered a distortion. Based on the obtained results, it can be stated that the additional output current vector generation has a slight influence on the THD distortions. It can be seen that under near rated motor load ($T_L \approx 0.8$ p.u.), THD values for stator current and voltage are below 1.5%.

Fig. 11 presents the stator current vector components in the first and second system planes. The shapes of the waveforms are almost circular. The visible oscillations result from the small value of the capacitance of the CSI output filter.

In Fig. 12, the rotor flux vector components in the stationary state are presented. The third harmonic is injected. The shape of the summarized rotor flux vector components $\psi_{r\alpha,\beta(1+2)}$ [see Fig. 12(a)] is almost trapezoidal. The trapezoidal shape of the rotor flux vector demonstrates that the magnetic circuit is better used, and hence, the electromagnetic torque of the drive system can be increased up to 12%–15% during the dynamic states [10].

B. FOC System

The FOC control system structure in which the third harmonic is possible to inject was presented in Fig. 4. The FOC control is well recognized in the literature on the presented subject; therefore, in this section, only the machine start-up to 1.0 p.u. and reverse to -1.0 p.u. are presented—the first and third harmonics are injected. In Fig. 13, the machine is starting up to 1.0 p.u. The rotor speed $\omega_{r(i)}$, electromagnetic torque $T_{e(i)}$, module of rotor flux vector $\psi_{rd(i)}$, and stator current vector components $i_{sd(i)}$ and $i_{sq(i)}$ are presented, where $i = 1,2$ for the first and second system plane, respectively. The response of electromagnetic torque

$T_{e(1)}$ is very quick—about 5 ms—however, while the rotor speed reaches the reference speed, the oscillations in $T_{e(1)}$ are visible. The visible coupling appears in the rotor flux module $\psi_{rd(1)}$, and in the change of the current $i_{sd(1)}$ value during the dynamic state. This indicates the lack of "complete" decoupling. In the control structure, there are only partial decouplings of the control paths. A similar situation appears while the IM is reversing to -1.0 p.u., which is shown in Fig. 14. During the crossing through the zero rotor speed, the rotor flux module changes its value about 0.05 p.u., which is visible in the waveform of the electromagnetic torque $T_{e(1)}$ [see Fig. 14(a)].

In Fig. 15, the stator current and stator voltage are presented during the five-phase machine start-up to 1.0 p.u. In Fig. 16, the stator current and stator voltage are presented during the five-phase machine reverse to 1.0 p.u. The registered stator current and voltages confirm that the third harmonic is injected and the rotor flux vectors are synchronized.

The dynamic properties of the FOC control structure in comparison to the proposed voltage approach (see Fig. 3) are similar; however, the control path is not fully decoupled—what is visible in Figs. 13 and 14—the state variables have a higher value of oscillations. The comparative study of the experimental results is presented in Section V-C.

C. Comparative Study of the Proposed Control Structures

The experimental results for the voltage control with the multiscalar variables were presented in Section V-A (control structure in Fig. 3), while the FOC control structure (see Fig. 4) has been presented in Section V-B. For these control structures, the third harmonic was injected. The tracking responses of the desired (actual) rotor speed are without overshoot for the cases, in which the machine was reversing as well as starting up to nominal speed (1.0 p.u.). For both cases, the torque rises quickly, showing the suitable effectiveness (about 5 ms). For both control system structures, the machine dynamic is comparable. However, the better quality of the waveforms is obtained for the voltage approach with the proposed multiscalar transformation (see Fig. 3). This is visible if the individual waveforms of the state variables are compared—for example, Figs. 5(a) and 6(a) to Figs. 13(a) and 14(a)—the waveforms for the FOC control system [see Figs. 13(a) and 14(a)] are more oscillated than the same variables for the voltage control scheme [see Figs. 5(a) and 6(a)]. In Figs. 13(a) and 14(a), the coupling between the electromagnetic and electromechanical subsystems is visible (during the dynamic states the rotor flux component $\psi_{rd(1)}$ has fluctuations of about 5% of nominal value). Similarly, the electromagnetic torque $T_{e(1)}$ [see Figs. 13(a) and 14(a)] is more oscillated than in Figs. 5(a) and 6(a) for the voltage control structure. However, in the stationary states, the tracking errors of controlled variables are minimized to zero for both considered cases, and the desired value is always kept. Similar situations occur for the state variables in the second system plane [see Figs. 5(b) and 6(b) to Figs. 13(b) and 14(b)]. In the case of the voltage control structure, the most important is variable K defined in (14), which is responsible for ensuring the suitable value of the current i_d in the dc link as well as coupling both system planes. Its waveforms are presented in Figs. 6 and 7. The comparison study is collected in Table I in which the chosen properties of the proposed control system schemes are presented. The comparison from Table I is not accurate, but "roughly" represents the properties of the proposed control structures with the FOC and state feedback control law with the multiscalar variables (see Figs. 3 and 4). The state feedback control structure (see Fig. 3) is characterized by the full decoupled stabilized control path and the smaller values of oscillations of the state variables than in the case of the FOC control structure. However, both control structures have a similar dynamic performance.

D. Comparison of Five-Phase CSI to the VSI Drive

The main advantage of the five-phase machine supplied by CSI is almost sinusoidal stator voltage and current. THD of stator current factor is smaller than 3% without load and for nominal load is about 1.2%. The THD of stator voltage is about 5.5% without load and 1.5% for the nominal load (see Table IV). In comparison to VSI, the THD of stator current is higher than 5% and about 3% for the nominal load (it is dependable on the modulation algorithm). However, to give the comparison, the VSI should be equipped with the output sinusoidal filter. In this case, the THD of stator current can be smaller than 1.5% for nominal machine load. The next advantage of the CSI drives is the possibility of a long cable connection of the machine and a small value of the stator voltage stress (*du/dt*) against the VSI. To obtain this in the VSI, it should possess the output filter. In sum, the CSI drives have one inductor in the dc link and the output capacitors, the VSIs (without output filter) have a smaller number of passive elements that makes their cost lower, and the chosen properties are worse. Considering the control and modulation algorithms, the VSIs are more popular than the CSI drives through this the modulation algorithms are better known in practical applications; however, the dead time of the transistors must be compensated. The control structure of the CSI drives is more complex and the simplest solutions (without the machine decoupling control) could provide to the undamped state variables. In both cases, it is possible to inject the third harmonic and better use the air-gap magnetic field to maximize the electromagnetic torque up to $2/\sqrt{3} \sim 1.155$ [10] (the maximum torque is increasing not in the whole range). It can be "said" that the maximum value of the square of stator current is $I^2_{s(1+2)} = I^2_{s(1)} + I^2_{s(2)} \approx 0.75$ and $I^2_{s(1)} \approx 0.85$ p.u., it is visible in Fig. 17. The summarized electromagnetic torque $T_{e(1+2)}$ is about 10% greater than the electromagnetic torque for $T_{e(1)}$ and the machine start-up to 0.9 p.u., for both harmonics generation, takes less time (about 40 ms) compared only to the first harmonic (only fundamental is generated). It is a visible benefit and confirms the verification of the proposed control scheme from Fig. 3 with the multiscalar transformation and the feedback control law of five-phase IM supplied by the CSI.

The biggest disadvantage of the CSI is the power electronic structure (diode in series connected to the transistor) and the lack of modules of these elements. This makes the CSI drives less popular than the VSI. Another drawback is the resonance problem in the CSI, which could appear between the output

capacitors and stator leakage inductance. In the open-phase of condition, the CSI is not robust as the VSI structure, in the CSI always two transistors conduct the current from dc link to the machine—so for the open of one or two stator phases, the modulation algorithm must be modified to not use these phases. Three transistors are always turned ON in the VSI. Therefore, the circuit of the stator current is not interrupted. The CSI drives are more beneficial than the VSI for high power multiphase motors, what was presented in [38]; however, there is the inverter structure with the thyristors and bulky choke in the dc link. The efficiency of the CSI is comparable to the VSI system—the output filter that was shown in [39]. The VSI without the output filter has the highest value of efficiency about 97% (it depends on the transistors).

VI. Conclusion

This article presents two control strategies of the five-phase IM supplied by the CSI. It was assumed that it is possible to generate the fundamental harmonic (in the first system plane) together with the third harmonic (in the second system plane). In the literature of the subject, we have not utilized the third-harmonic injection in the drive system supplied by the CSI. From this point of view, the proposed solution in this article is the new approach, especially the control strategy with the multiscalar linearization and the state feedback control law with the control variables ($e_{d(1)}$, $\omega_{if(1)}$) and ($e_{d(2)}$, $\omega_{if(2)}$) for the introduced "virtual" dc-link circuit. The control strategy presented in this article allows controlling the state variables of IM in the first and the second system planes independently. The experimental results confirmed that the both control strategies are suitable for application in the drive system with the five-phase IM supplied by the CSI. Better properties of the IM, visible on the example of presented state variables, are achieved if the multiscalar transformation was used, although the dynamic of the IM is on the same level (see Table I). In this case, by using the multiscalar transformation and the state feedback control law, it is possible to obtain full drive system linearization (the dc link–machine–the output filter capacitor). This is important in the drive system supplied by the CSI because, if the control variables are not adequate, the resonance problems occur between the machine leakage inductance and the filter capacitors. On a small scale, it is visible in the FOC control system presented in the experimental results in Section V-B (higher oscillation in the transients T_e, i_{sq} and i_{sd}). This problem was indicated in [24] and [25] for three-phase IM. In the case of multi (five) phase machines the control system is more complex than for a three-phase; therefore, it is recommended to use a suitable control strategy to prevent these unfavorable effects. The proposed two control structures of the five-phase machine supplied by the CSI are the main contribution of this article.

The control strategy presented in this article, dedicated to multiphase machines supplied by the CSI, can be used in different industrial applications: electric ship propulsion, locomotive traction, compressors, electric aircraft systems, and electromobility.

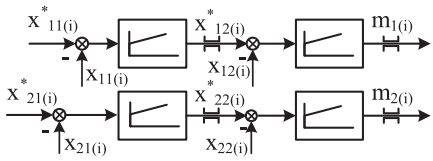

Fig. 18. Internal connection of PI-controllers structure (according to introduced in Section III markings).

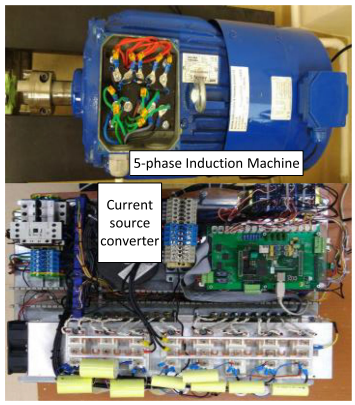

Fig. 19. Experimental stand photograph.

The transistor modulation algorithm, common-mode current, and voltage as well as reliability in the fault states are not considered in this article.

Appendix

In the control system scheme presented in Fig. 3, there are the first system plane blocks with the PI-controllers structure. This structure is presented in Fig. 18. For the second system plane, the PI-controller of $x_{11(2)}$ does not exist and the value of $x*_{12(2)}$ is determined from (49), which is another advantage compared to the FOC control structure (see Fig. 4) and the synchronization method [9]–[15], [33].

Table II tabulates tuning gains of PI-controllers presented in Fig. 18, where k_p with index 11…22 means the PI-controller gains variable from Fig. 18, ($k_{p\omega}$, $k_{i\omega}$) and ($k_{p\psi r}$, $k_{i\psi r}$) are the gains of PI-controllers in the FOC control system [28].

In Table III, the nominal parameters of an electric drive system with IM supplied by the CSI are tabulated.

In Fig. 19, the photograph of the experimental stand with the current source converter and 5.5 kW five-phase squirrel-cage induction machine is shown. The interface with the DSP processor with the extension board are visible, three transistors bridge with diodes (MMG50SR120FZB) for the current source rectifier as well as five transistors bridge for the CSI, the input and output capacitors and the inductor in the dc link.

References

[1] E. Levi, R. Bojoi, F. Profumo, H. A. Toliyat, and S. Williamson, "Multiphase induction motor drives - A technology status review," *IET Electron. Power Appl.*, vol. 1, no. 4, pp. 489–516, 2007, doi: 10.1049/iet-epa:20060342.

[2] C. S. Lim, E. Levi, and M. Jones, "FCS-MPC-based current control of a five-phase induction motor and its comparison with PI-PWM control," *IEEE Trans. Ind. Electron.*, vol. 61, no. 1, pp. 149–163, Feb. 2014.
[3] F. Barrero, S. Member, and M. J. Duran, "Recent advances in the design, modeling and control of multiphase machines – Part 1," *IEEE Trans. Ind. Electron.*, vol. 63, no. 1, pp. 449–458, Jun. 2016.
[4] M. J. Duran and F. Barrero, "Recent advances in the design, modeling and control of multiphase machines – Part 2," *IEEE Trans. Ind. Electron.*, vol. 63, no. 1, pp. 459–468, Jan. 2016.
[5] L. Parsa and H. Toliyat, "Five-phase permanent magnet motor drives for ship propulsion applications," in *Proc. IEEE Electr. Ship Technol. Symp.*, Jul. 2005, pp. 371–378.
[6] E. Levi, F. Barrero, and M. J. Duran, "Multiphase machines and drives – revisited," *IEEE Trans. Ind. Electron.*, vol. 63, no. 1, pp. 426–432, Oct. 2016.
[7] A. S. Abdel-Khalik, M. I. Masoud, and B. W. Williams, "Improved flux pattern with third harmonic injection for multiphase induction machines," *IEEE Trans. Power Electron.*, vol. 27, no. 3, pp. 1563–78, Aug. 2012.
[8] M. Salehifar, R.S. Arashloo, and M. Moreno-Eguilaz, "Observer based open transistor fault diagnosis and fault tolerant control of five-phase permanent magnet motor drive for application in electric vehicle," *IET Power Electron.*, vol. 8, no. 1, pp. 76–87, 2015.
[9] H. Xu, H. Toliyat, and L. Petersen, "Rotor field oriented control of five-phase induction motor with the combined fundamental and third harmonic currents," in *Proc. 16th Annu. IEEE Appl. Power Electron. Conf. Expo.*, 2001, vol. 1, pp. 392–398.
[10] M. Mengoni, L. Zarri, A. Tani, L. Parsa, G. Serra, and D. Casadei, "High-torque-density control of multiphase induction motor drives operating over a wide speed range," *IEEE Trans. Ind. Electron.*, vol. 62, no. 2, pp. 814–825, Jul. 2015.
[11] L. Zheng, J. E. Fletcher, B. W. Williams, and X. He, "Dual-plane vector control of a five-phase induction machine for an improved flux pattern," *IEEE Trans. Ind. Electron.*, vol. 55, no. 5, pp. 1996–2005, Apr. 2008.
[12] F. Wilczynski, M. Morawiec, P. Strankowski, J. Guziński, and A. Lewicki, "Sensorless field oriented control of five phase induction motor with third harmonic injection," in *Proc. IEEE 11th Int. Conf. Compat., Power Electron. Power Eng.*, Apr. 2017, pp. 392–397.
[13] H. Echeikh, R. Trabelsi, A. Iqbal, N. Bianchi, and M. F. Mimouni, "Non-linear backstepping control of five-phase IM drive at low speed conditions–experimental implementation," *ISA Trans.*, vol. 65, pp. 244–253, 2016.
[14] H. Echeikh, R. Trabelsi, A. Iqbal, N. Bianchi, and M. F. Mimouni, "Comparative study between the rotor flux oriented control and non-linear backstepping control of a five-phase induction motor drive – An experimental validation," *IET Power Electron.*, vol. 9, no. 13, pp. 2510–2521, 2016.
[15] B. Khaldi, H. Abu-Rub, and A. Iqbal, "Sensorless direct torque control of five-phase induction motor drives," in *Proc. 37th Annu. Conf. IEEE Ind. Electron. Soc.*, Nov. 2011, pp. 3501–3506.
[16] A. Tabrizchi, J. Soltani, and J. Shishehgar, "Direct torque control of speed sensorless five-phase IPMSM based on adaptive input-output feedback linearization," in *Proc. 5th Conf. Power Electron., Drive Syst. Technol.*, 2014, pp. 43–48.
[17] J. Chiasson, "Dynamic feedback linearization of the induction motor," *IEEE Trans. Automat. Control*, vol. 38, no. 10, pp. 1588–1594, Oct. 1993.
[18] M. Morawiec, P. Strankowski, A. Lewicki, J. Guziński, and F. Wilczyński, "Feedback control of multiphase induction machines with backstepping technique," *IEEE Trans. Ind. Electron.*, vol. 67, no. 6, pp. 4305–4314, Jun. 2020.
[19] B. R. Pelly, *Thyristor Phase-Controlled Converters and Cycloconverters*. New York, NY, USA: Wiley, 1971.
[20] C. Klumpner and F. Blaabjerg, "Using reverse-blocking IGBTs in power converters for adjustable-speed drives," *IEEE Trans. Ind. Appl.*, vol. 42, no. 3, pp. 807–816, Jun. 2006.
[21] Y. Xu, Z. Wang, P. Liu, Q. Song, C. Tang, and M. Cheng, "Zero-voltage-switching current-source-inverter motor drives based on silicon carbide devices," in *Proc. 22nd Int. Conf. Electron. Mach. Syst.*, 2019, pp. 1–5.
[22] B. Sahan, S. V. Araújo, C. Noding, and P. Zacharias, "Comparative evaluation of three-phase current source inverters for grid interfacing of distributed and renewable energy systems," *IEEE Trans. Power Electron.*, vol. 26, no. 8, pp. 2304–2318, Aug. 2011.
[23] R. Ryndzionek and Ł. Sienkiewicz, "Evolution of the HVDC link connecting offshore wind farms to onshore power systems," *Energies*, vol. 13, no. 8, pp. 1–10, 1914, doi: 10.3390/en13081914.
[24] M. Salo and H. Tusa, "Vector-controlled PWM current-source-inverter-fed induction motor drive with a new stator current control method," *IEEE Trans. Ind. Electron.*, vol. 52, no. 2, pp. 523–531, Apr. 2005.
[25] A. B. Nikolic and B. I. Jeflenic, "Direct torque control and virtual-flux based direct power control of current source converter in wind turbine application," in *Proc. 14th Eur. Conf. Power Electron. Appl.*, 2011, pp. 1–10.
[26] M. Morawiec, Z. Krzeminski, and A. Lewicki, "Voltage multiscalar control of induction machine supplied by current source converter," in *Proc. IEEE Int. Symp. Ind. Electron.*, Jul. 2010, pp. 3119–3124.
[27] M. Morawiec, F. Wilczynski, and A. Lewicki, "Control of induction machine supplied by a current source inverter using the multi-scalar transformation and backstepping approach," in *Proc. 19th Eur. Conf. Power Electron. Appl.*, 2017, pp. 1–10.
[28] M. A. Elgenedy, A. S. Abdel-Khalik, A. M. Massoud, and S. Ahmed, "Indirect field oriented control of five-phase induction motor based on SPWM-CSI," in *Proc. Int. Conf. Electron. Mach.*, 2014, pp. 2101–2106.
[29] M. A. Elgenedy, A. S. Abdel-Khalik, S. Ahmed, and A. M. Massoud, "Sinusoidal PWM modulation technique of five-phase current-source-converters with controlled modulation index," in *Proc. IEEE Int. Symp. Ind. Electron.*, Jun. 2014, pp. 655–660.
[30] M. A. Elgenedy, A. Mohamed, A. A. Elserougi, A. S. Abdel-Khalik, A. M. Massoud, and S. Ahmed, "A space vector PWM scheme for five-phase current-source converters," *IEEE Trans. Ind. Electron.*, vol. 63, no. 1, pp. 562–573, Oct. 2015.
[31] S. M. Dabour, M. F. Elmorshedy, and E. M. Rashad, "Generalized SVM technique for multiphase current source inverters," in *Proc. 20th Int. Conf. Electron. Mach. Syst.*, 2017, pp. 1–6.
[32] R. Marino, P. Tomei, and C.M. Verrelli, "Induction machine control design," in *Advance in Industrial Control*. London, U.K.: Springer, 2010, doi: 10.1007/978-1-84996-284-1.
[33] L. Zheng, J. E. Fletcher, B. W. Williams, and X. He, "Dual-plane vector control of a five-phase induction machine for an improved flux pattern," *IEEE Trans. Ind. Electron.*, vol. 55, no. 5, pp. 1996–2005, May 2008.
[34] M. Adamowicz, Z. Krzemiński, M. Morawiec, P. Strankowski, and J. Guziński, "Five phase induction motor multiscalar control," *Przeglad Elektrotechniczny*, vol. 92, no. 5, pp. 106–113, 2016.
[35] M. Morawiec, "Z-type observer backstepping for induction machines," *IEEE Trans. Ind. Electron.*, vol. 62, no. 4, pp. 2090–2103, Sep. 2015.
[36] Z. Krzeminski, "Nonlinear control of induction motor," in *Proc. 10th IFAC World Congr.*, 1987, pp. 349–354.
[37] P. S. N. De Silva, J. E. Fletcher, and B. W. Williams, "Design of a five-phase induction motor using flux distribution optimisation," in *Proc. 3rd IET Int. Conf. Power Electron., Mach. Drives*, 2006, pp. 331–335.
[38] S. Castellan, G. Sulligoi, and A. Tessarolo, "Comparative performance analysis of VSI and CSI supply solutions for high power multi-phase synchronous motor drives," in *Proc. Int. Symp. Power Electron., Electron. Drives, Automat. Motion*, 2008, pp. 854–859.
[39] S. Narasimhan, A. Anurag, and S. Bhattacharya, "Comparative study of a 3.3 kV SiC-based voltage and current source inverter for high-speed motor drive applications," in *Proc. IEEE 12th Energy Convers. Congr. Expo. Asia*, 2021, pp. 2211–2217.

Marcin Morawiec (Senior Member, IEEE) received the M.Sc. degree in electrical engineering from the Czestochowa University of Technology, Czestochowa, Poland, in 2003, and the Ph.D. and D.Sc. degrees from the Gdansk University of Technology, Gdansk, Poland, in 2007 and 2017, respectively.

Since 2017, he has been an Associate Professor with the Gdansk University of Technology. He is the author of more than 95 articles and 2 monographs and 2 chapters in books, 1 Polish patent, and 5 patent applications. His main scientific activities are concentrated on multiscalar models, nonlinear control of any electrical machines, sensorless control, nonlinear control, backstepping control, adaptive observer backstepping, and sliding mode control.

Filip Wilczyński received the M.Sc. degree from the Faculty of Electrical Engineering, Gdansk University of Technology, Gdansk, Poland, in 2016, and the Ph.D. degree from the Gdansk University of Technology, Gdansk, Poland, both in electrical engineering.

His research interests include nonlinear control of electric drives, multiphase machines, sensorless control, and current-source inverters.